MAX-PLANCK-INSTITUT FÜR PLASMAPHYSIK

GARCHING BEI MÜNCHEN

LOWER-HYBRID-RESONANCE HEATING OF A PLASMA IN A PARALLEL-PLATE WAVEGUIDE

S. Puri and M. Tutter

IPP IV/37 June 1972

Die nachstehende Arbeit wurde im Rahmen des Vertrages zwischen dem Max-Planck-Institut für Plasmaphysik und der Europäischen Atomgemeinschaft über die Zusammenarbeit auf dem Gebiete der Plasmaphysik durchgeführt.

IPP IV/37 S. Puri
M. Tutter

Lower-Hybrid-Resonance Heating of a Plasma in a Parallel-Plate Waveguide

June 1972 (in English)

Abstract

Wave propagation in a parallel-plate metallic waveguide partially filled with an inhomogeneous, anisotropic plasma column is studied as an eigenvalue problem using the complete cold-plasma dielectric tensor. Although the accessibility condition is not met, the collisional energy absorption at the lower-hybrid resonance greatly exceeds the resistive loss at the waveguide walls resulting in a very high plasma heating efficiency. The bulk of the wave energy dissipated goes into heating the electrons. The heating continues to be effective even for very low cillision frequencies encountered in thermonuclear plasmas. Detailed numerical results for the heating efficiency, energy flux into the plasma, energy density and dissipation density in the plasma column as well as group velocity are presented. Also the effects of density profile, collision frequency, and waveguide eigenmodes are discussed.

I. INTRODUCTION

An electromagnetic wave incident upon an inhomogeneous, cold-plasma column gradually converts into a slow electrostatic wave. If the plasma density is high enough, the wave eventually encounters a region of very high refractive index and low group velocity in the vicinity of the lower-hybrid resonance. As early as 1955, Budden predicted complete absorption of such waves at the singular turning point [1, 2]. These effects have been extensively studied in ionospheric propagation as well as for plasma heating in the laboratory and the effectiveness of transferring rf energy into the plasma at the lower-hybrid-resonance (LHR) is well established [3, 11].

The launching mechanisms hitherto considered are i) electromagnetic waves approaching from infinity [10], ii) excitation with "Stix coil" [7] allowing an arbitrary choice of k_z, iii) coupling with a plasma capacitor [9] or iv) gap excitation which couples most of the spectral energy in wave numbers such that the refractive index $n_z > 1$ thereby fulfilling the accessibility condition [8].

In this paper we extend the analysis to include the effect of metallic walls with a finite conductivity [1,2]. Apart from the obvious interest of such a configuration, free from any structure whatsoever, from the fusion standpoint, several disturbing features in the lower-hybrid (LH) heating studies are automatically obviated. The problem of selecting a particular

angle of incidence does not arise because k_z, the propagation constant in the magnetic field direction is uniquely specified in the eigenvalue solution. Similarly, the obscuring effects of geometric resonances [7, 10] are inherently absent. Also, it is possible to calculate the heating efficiency by a direct comparison of energy deposited in the plasma with the wall dissipation.

The absorption mechanism considered is the momentum transfer collisions between the electrons and ions using the Langevin model [3]. Departing from the usual practice of stepwise numerical solution of the wave equation using coupled, linear differential equations, we shall employ a stratified plasma model. This model becomes exact as the number of slabs tends to infinity and the thickness of each slab approaches zero. In practice, an acceptable approximation is obtained by making each plasma slab much thinner than the local value of the wavelength.

Beyond the inaccuracies inherent in the Langevin collision model and the stratification of the plasma profile, the problem can be treated exactly. For the four plasma waves occuring in each slab, four boundary conditions exist requiring the continuity of the tangential electric and magnetic fields.

In Sec. II the general method of solution is outlined. Section III treats in detail a representative case. In Sec. IV the effects of varying the parameters is considered. Some of the computational problems encountered are discussed in Sec. V. The significance of the results and their comparison with the existing theories is discussed in Sec. VI.

Unless otherwise specified, the units used are rationalized MKS. All field quantities are assumed to posses space and time dependence exp $i(k_x x + k_z z - \omega t)$ with no variation in the y-direction. We choose ω to be real, while k_x and k_z are allowed to assume complex values.

II. THE METHOD OF SOLUTION

The parallel-plate plasma filled waveguide as well as the electric field configuration (dashed lines) for a symmetric propagating eigenmode are shown in Fig.1a. The stratified trapezoidal plasma density profile with S steps on each side of the axis and consequently with a total of (2S-1) plasma slabs is shown in Fig.1b. The full cold plasma dielectric tensor used in a plasma slab of uniform electron density n_e is,

$$K = \begin{pmatrix} K_\perp & -iK_x & 0 \\ iK_x & K_\perp & 0 \\ 0 & 0 & K_{\parallel} \end{pmatrix}$$

where

$$K_\perp = 1 - \frac{\omega_{pi}^2}{\omega^2 - \omega_{ci}^2} - \frac{\omega_{pe}^2}{\omega^2 - \omega_{ce}^2}$$

$$K_x = \frac{\omega_{ci}}{\omega} \frac{\omega_{pi}^2}{\omega^2 - \omega_{ci}^2} - \frac{\omega_{ce}}{\omega} \frac{\omega_{pe}^2}{\omega^2 - \omega_{ce}^2}$$

$$K_{\parallel} = 1 - \frac{\omega_{pi}^2}{\omega^2} - \frac{\omega_{pe}^2}{\omega^2}$$

$$\omega_{pi}^2 = \frac{n_e e^2}{M \epsilon_0}, \quad \omega_{pe}^2 = \frac{n_e e^2}{m_e \epsilon_0}, \quad \omega_{ci} = \frac{e B_0}{M}$$

and $$\omega_{ce} = \frac{e B_o}{m_\nu} .$$

In conformity with the use of the Langevin equation, m_ν in the above equations is defined as

$$m_\nu = m(1 - i \nu_{ei}/\omega)$$

where m is the electron mass and ν_{ei} is the electron-ion momentum transfer collision frequency according to Spitzer [14]. We shall often specify ν_{ei} by the equivalent temperature T. This would lead to a variable value of ν_{ei} across the inhomogeneous plasma column. It should, however, be remembered that apart from specifiying ν_{ei}, T does not imply any departure from the cold plasma theory.

Defining $\tilde{K}_\perp = K_\perp - n_z^2$, the dispersion relation may be written as,

$$n_x^2 = \frac{K_\perp \tilde{K}_\perp - K_x^2 + K_{||} \tilde{K}_\perp}{2 K_\perp} \pm \sqrt{\left(\frac{K_\perp \tilde{K}_\perp - K_x^2 + K_{||} \tilde{K}_\perp}{2 K_\perp} \right)^2 + \frac{K_{||}}{K_\perp} \left(K_x^2 - K_\perp^2 \right)}$$

Corresponding to the four roots of this equation, the fields associated with the four waves in a given plasma slab are

$$E_{x\pm}^{f,s} = \hat{E}_{x\pm}^{f,s} \exp i\left(k_{x\pm}^{f,s} x + k_z z - \omega t \right)$$

$$E_{y\pm}^{f,s} = \frac{i K_x}{\left(n_{x\pm}^{f,s} \right)^2 + n_z^2 - K_\perp} E_{x\pm}^{f,s} .$$

$$E_{z\pm}^{f,s} = \frac{n_{x\pm}^{f,s}\, n_z}{(n_{x\pm}^{f,s})^2 - K_{11}} E_{x\pm}^{f,s}$$

$$H_{x\pm}^{f,s} = -n_z E_{y\pm}^{f,s} / \eta_o$$

$$H_{y\pm}^{f,s} = \left(- n_{x\pm}^{f,s} E_{z\pm}^{f,s} + n_z E_{x\pm}^{f,s}\right) / \eta_o$$

$$H_{z\pm}^{f,s} = n_{x\pm}^{f,s} E_{y\pm}^{f,s} / \eta_o$$

where the capped field quantities denote the complex amplitudes, and η_o is the vacuum impedance $(\mu_o/\varepsilon_o)^{1/2}$. The indices f (fast) and s (slow) correspond to the smaller and the larger roots of n_x^2, respectively. For each of the roots n_x^2 the two waves associated with $\pm n_x$ are labeled plus and minus, respectively, so that $n_{x+} = -n_{x-}$. The slow wave is the quasi-extraordinary mode which encounters the resonance at the LH layer as $K_\perp \rightarrow 0$. Depending upon the choice of symmetric or an antisymmetric waveguide mode $E_{x+}^{f,s} = \mp E_{x-}^{f,s}$ in the central plasma slab so that there are only two instead of four undetermined amplitudes in this slab.

In the vacuum region there exist two TE modes

$$E_{y\pm}^{TE} = \hat{E}_{y\pm}^{TE} \exp i\left(\pm k_{xo} x + k_z z - \omega t\right)$$

$$H_{x\pm}^{TE} = -n_z E_{y\pm}^{TE} / \eta_o$$

$$H_{z\pm}^{TE} = \pm\left(1 - n_z^2\right) E_{y\pm}^{TE} / \eta_o$$

and two TM modes

$$H_{y\pm}^{TM} = \hat{H}_{y\pm}^{TM} \exp i(\pm k_{xo} x + k_z z - \omega t)$$

$$E_{x\pm}^{TM} = n_z H_{y\pm}^{TM} \eta_o$$

$$E_{z\pm}^{TM} = \mp (1 - n_z^2) H_{y\pm}^{TM} \eta_o$$

where k_{xo}, the propagation constant in vacuum is given by $k_{xo}^2 + k_z^2 = k_o^2 = \omega^2/c^2$.

Finally, the two outgoing waves in the metallic wall are

$$E_{yw}^{TE} = \hat{E}_{yw}^{TE} \exp i(-k_{xw} x + k_z z - \omega t)$$

$$H_{xw}^{TE} = -n_z E_{yw}^{TE} / \eta_o$$

$$H_{zw}^{TE} = -(1 - n_z^2) \varsigma E_{yw}^{TE} / \eta_o$$

and

$$H_{yw}^{TM} = \hat{H}_{yw}^{TM} \exp i(-k_x w + k_z z - \omega t)$$

$$E_{xw}^{TM} = n_z \varsigma H_{yw}^{TM} \eta_o$$

$$E_{zw}^{TM} = (1 - n_z^2) \varsigma \xi H_{yw}^{TM} \eta_o$$

where

$$\zeta = \pm \left[1 + \frac{i\sigma}{\omega \epsilon_o (1 - n_z^2)} \right]^{1/2}$$

$$\xi = \left[1 + \frac{i\sigma}{\omega \epsilon_o} \right]^{-1}$$

$$k_{xw} = k_o (1 - n_z^2) \zeta$$

and σ is the wall conductivity. Care should be exercised in selecting the sign of ζ in order that the waves decay, away from the waveguide axis, there being no sources at infinity.

Remembering that n_z itself is unknown, one can readily verify that the number of undetermined quantities (wave amplitudes and n_z) exactly equals the number of boundary conditions (including the symmetry or asymmetry condition) plus the additional available constraint for normalizing the field amplitudes. The normalization used throughout this paper is that the vacuum electric field component $(E_x)_{z=o} \equiv 1$ Volt/cm just outside the vacuum plasma interface.

The resultant set of algebraic linear, transcendental equations is solved using standard iteration techniques. In general several solutions are found, each being an eigenmode with the associated eigenvalue n_z. Once n_z is determined all other quantities of interest can be readily calculated.

III. THE REPRESENTATIVE CASE

Table I summarizes the parameters used in the representative case which will be studied in detail in this section. The choice of waveguide dimensions, magnetic field and plasma parameters is made so that several propagating modes can exist simultaneously. Since the Langevin equation is an approximation, the inclusion of collisions should not considerably alter the dielectric co-efficient in order to maintain the credibility of the results obtained. A very low collision rate, on the other hand, produces too thin an absorption layer to allow a satisfactory protrayal of the results by means of figures. Hence, a compromise temperature of 3×10^4 ^oK corresponding to an average relative collision frequency $\langle \nu_{ei} \rangle / \omega \simeq 10^{-2}$ is selected. The number of plasma slabs has to be restricted to 199 by considerations of the computer capacity. In order that the slab model be an accurate representation of a smoothly varying profile, it is necessary that the total phase change $\Delta\phi = |k_x^s \Delta x| << 2\pi$ in each of the slabs. By choosing the plasma-profile width $g = 1$ cm it is possible to keep $\Delta\phi/2\pi < 1/30$ and, as we shall see later, leads to an acceptable accuracy of the results.

We proceed to present the detailed results obtained for the prarmeters listed in Table I.

a) HEATING EFFICIENCY AND ABSORPTION LENGTH

In Table II the eigenvalues n_z for five propagating eigenmodes of the waveguide are given. The absorption length defined by

$$\lambda_{abs} = \left[Im\,(k_z) \right]^{-1}$$

is typically of the order of several meters. The power dissipation density in the plasma is given by the divergence of the Poynting vector

$$P_{diss} = - \nabla \cdot \frac{1}{2} (E \times H^*)$$

where the asterik denotes complex conjugation. Both the heating efficiency

$$\eta = \frac{\int_{-a}^{a} P_{diss}(x)\, dx}{\int_{-\infty}^{\infty} P_{diss}(x)\, dx}$$

and average power dissipation in the plasma

$$\langle P_{diss} \rangle = \frac{1}{a} \int_{0}^{a} P_{diss}(x)\, dx$$

at z = o are also given in Table II.

It is seen that both $\langle P_{diss} \rangle$ and η are higher for the eigenmodes with smaller value of n_z. In the remainder of this section we shall confine our attention to the mode

with the largest value of the refractive index n_z with the tacit knowledge that still more favourable results may be expected with other modes.

b) THE ELECTRIC FIELD

As the hybrid-resonance is approached, the wavelength of the slow wave decreases while its amplitude increases and E_x reaches a maximum value of over 3oo times the vacuum electric field (Fig.2). The peculiar distortion in the curves is due to the cubic compression of the vertical scale. At the same time, the wave becomes progressively electrostatic with an ever decreasing angle between the propagation vector and the electric field (Fig.3).

The fast wave, on the contrary, remains oblivious of the catastrophic events occuring at the hybrid layer.

c) DISSIPATION AND ENERGY DENSITIES

Dissipation (shown in Fig.4 as a function of position) per unit volume of the plasma is given by

$$P_{diss} = -\nabla \cdot \frac{1}{2} (E \times H^*)$$

$$= -\frac{i}{2} \left[E_y \left\{ k_x^f \left(H_{z-}^f - H_{z+}^f \right) + k_x^s \left(H_{z-}^s - H_{z+}^s \right) \right\}^* \right.$$

$$+ H_z^* \left\{ k_x^f \left(E_{y+}^f - E_{y-}^f \right) + k_x^s \left(E_{y+}^s - E_{y-}^s \right) \right\}$$

$$+ H_y^* \left\{ k_x^f \left(E_{z-}^f - E_{z+}^f \right) + k_x^s \left(E_{z-}^s - E_{z+}^s \right) \right\}$$

$$+ E_z \left\{ k_x^f \left(H_{y+}^f - H_{y-}^f \right) + k_x^s \left(H_{y+}^s - H_{y-}^s \right) \right\}^*$$

$$+ \left(k_z - k_z^* \right) \left(E_x H_y^* - E_y H_x^* \right) \Big]$$

where the field quantities without a superscript denote total field due to all the four waves and $k_x^{f,s} = k_{x+}^{f,s}$. As expected, dissipation occurs in a very narrow region. Over 9o % of the energy is absorbed in a width no greater than 4/1o of a millimeter, thus underlining the local character of LH-heating.

The energy density of the plasma may be written as

$$\mathcal{E} = \frac{1}{4} \left[\epsilon_o E^* \cdot \frac{\partial}{\partial \omega} (\omega K) \cdot E + \mu_o H^2 \right]$$

$$= \frac{\epsilon_o}{4} \Big[(K_\perp + \omega K_\perp') (E_x^2 + E_y^2) + i (K_x + \omega K_x') (E_x E_y^* - E_x^* E_y)$$

$$+ (K_\parallel + \omega K_\parallel') E_z^2 \Big] + \frac{\mu_o}{4} \left(H_x^2 + H_y^2 + H_z^2 \right)$$

where $H^2 \equiv H \cdot H^*$, and $K_\perp' = \frac{\partial K_\perp}{\partial \omega}$, etc. By expressing K as a sum of vacuum, electron and ion components, it is possible to calculate the energy density associated with each of the particle species. Both $\mathcal{E}$ and the ratio of ion to the total energy density $\mathcal{E}_i / \mathcal{E}$ are shown in Fig.5. Contrary to expectations, ions carry only half of the wave energy even at the resonance. This curious phenomenon is due to the subtle but important effect of the small longitudinal electric field E_z which due to the large value of the parallel component of the dielectric

tensor $K_{\parallel}$ for the electrons, imparts them an energy density comparable to the ion energy derived from the much larger transverse electric fields.

d) GROUP VELOCITY AND ENERGY PENETRATION TIME

From the dispersion relation, one obtains by partial differentation, the group velocities

$$v_{gx}^{f,s} = \frac{\partial \omega}{\partial k_x^{f,s}} = \frac{1}{k_o} \frac{P}{Q}$$

and

$$v_{gz} = \frac{\partial \omega}{\partial k_z} = \frac{1}{k_o} \frac{R}{S}$$

where (the superscript f,s has been dropped),

$$P = 4 n_x^3 K_\perp + 2 n_x \left[K_x^2 - (K_\parallel + K_\perp)(K_\perp - n_z^2) \right]$$

$$Q = n_x^2 K_\perp' \left[- n_x^2 + K_\parallel + (K_\perp - n_z^2)(1 - K_\perp - 2K_\parallel) \right]$$
$$+ K_\parallel' \left[(K_\perp - n_z^2)(n_x^2 - K_\perp + n_z^2) + K_x^2 \right]$$
$$+ 2 K_x K_x' \left[K_\parallel - n_x^2 \right]$$

$$R = 4 n_z^3 K_\parallel + 2 n_z \left[n_x^2 (K_\parallel + K_\perp) - 2 K_\parallel K_\perp \right]$$

$$S = K_\perp' \left[n_z^2 (K_{11} - n_x^2) + K_{11} n_z^2 - (K_{11} - n_x^2)(K_\perp - n_x^2 - K_x^2) - K_\perp (K_{11} - n_x^2) \right]$$
$$+ K_{11}' \left[- n_z^4 + K_\perp n_z^2 + (K_\perp - n_x^2) n_z^2 - K_\perp (K_\perp - n_x^2 - K_x^2) \right]$$
$$+ 2 K_x K_\perp K_x' \left[K_{11} - n_x^2 \right]$$

The ratio of group velocity to the light velocity in vacuum is plotted as a function of position in Fig.6. Surprisingly enough, not only v_{gx} but also v_{gz} for the slow wave become much smaller than the light velocity near the LH resonance.

In Fig.7 the actual propagation of an energy pulse (travelling at the group velocity of the slow wave) from the plasma boundary to the hybrid layer is shown as a function of elapsed time. The time (25 μsec in this case) that the energy pulse requires to travel to the absorption region from the vacuum (where the energy source will be actually located in an experiment) is a measure of the interval necessary for establishing steady-state conditions and for observing heating effects in the plasma. We shall refer to this characteristic interval as the penetration time τ_{pen}.

IV. VARYING THE PARAMETERS

In this section we study the effect of changing the density profile, rf frequency and collision frequency on the heating efficiency and average energy dissipation.

a) THE DENSITY PROFILE

Fig.8 shows the average power dissipation density and the heating efficiency as the profile width "g" is changed from o.5 cm to 3.5 cm. The dip at g = 2 cm is presumably because the LHR, where most of the absorption occurs, lies at the field minima (A in Fig.1a) of the eigenmode for this particular choice of g.

Instead of linear, the plasma density profile was made in turn flat topped sinusoidal

$$|X| = \left[\cos^{-1}\left(\frac{2n_e}{n_{max}} - 1\right) - \pi\right] / \pi + X_o$$

and flat topped parabolic

$$|X| = \sqrt{n_e / n_{max}} + X_o$$

respectively, where x_o is a reference axis. There was a slight increase in the power dissipation in the former case and a similar decrease in the latter. Neither of these changes

are significant, however, and we may safely assume that the LH heating is rather insensitive to the precise delineation of the density profile.

Changing the plasma column width "2a" as well as introducing a thin plasma in the vacuum region does not much alter the results either.

b) RF FREQUENCY

Fig.9 shows $\langle P_{diss} \rangle$ and η as a function of the applied frequency. A bump reminiscent of the dip in the previous section (IVa) occurs when the LHR lies at the field maxima (B in Fig.1a) of the eigenmode. The observations of this and the previous section, however, are not to be confused with "geometrical resonances" [7, 10] occuring when the plasma column is not contained inside a waveguide.

c) COLLISION FREQUENCY

As the collision frequency is lowered (or T increased) both η and $\langle P_{diss} \rangle$ pass through a maximum and then decrease monotonically (Fig.1o). It is a matter of some surprise that even for $\langle \nu_{ei} \rangle / \omega$ as low as 10^{-7} there is appreciable collisional energy absorption at the LHR.

Predictably enough the absorption layer gets thinner while the maximum value attained by E_x becomes larger. The time required for the energy pulse to arrive at the hybrid layer from the vacuum region also increases.

In a sense, the results reported for high temperatures become academic because it would be difficult, in practice, to produce low enough electric fields in the vacuum region so as to fulfill the requirements of a linearized treatment in the vicinity of the resonance.

V. COMPUTATIONAL PROBLEMS AND CHECKS ON ACCURACY

a) COMPUTATIONAL PROBLEMS

In the neighbourhood of the resonance $|Im(k_{xs})| \gg 1$ and quantities like $\exp\left[i\ (k_{xs}x)\right]$ create computer overflow problems. This difficulty can be circumvented by transforming the axis x = o to the hybrid layer during the computational phase.

In order to have the maximum accuracy with the given number of plasma slabs, it is desirable that the phase change in each slab of width Δx

$$|\Delta\phi| = |k_x^s|\ \Delta x$$

be approximately equal. Initially the slab thicknesses are roughly assigned and $\phi = \sum |\Delta\phi|$ and n_z are computed. In the final computation new slab widths $\Delta x = \phi/S\ |k_{xs}|$ are assigned, taking care that the maximum plasma density in the center of the column remains unchanged.

b) CHECKS ON ACCURACY OF COMPUTATIONS

Following checks on computation accuracy were found to be true with an accuracy of better than one part in a thousand.

i) Continuity of the Poynting Vector - Since the tangential electric and magnetic fields are continuous across the boundary, the normal component, $1/2\ (E_y H_z^* - E_z H_y^*)$ of the Poynting vector must also be continuous across each boundary.

ii) Continuity of Electric Displacement and Magnetic Induction - The continuity of the tangential components of the electric and magnetic fields automatically imply that

$$D_x = \epsilon_0 (K_\perp E_x - i K_x E_y)$$

and

$$B_x = \mu_0 H_x$$

be continuous at each boundary.

iii) Equality of Dissipation Density with the Divergence of the Poynting Vector - By far the most stringent test involves establishing in each plasma slab the equality of divergence of the Poynting vector (see Sec. IVc and Fig.4) with the rate of change of energy density given by

$$-\frac{i\omega}{2}\left[\mu_0 H^2 - \epsilon_0 (E^* \cdot K \cdot E)^*\right]$$

$$= -\frac{i\omega}{2}\left[\mu_0 H^2 - \epsilon_0 \left\{K_\perp (E_x^2 + E_y^2) + i K_x (E_x E_y^* - E_x^* E_y) + K_{11} E_z^2 \right\}\right] .$$

c) ACCURACY OF THE STRATIFIED PLASMA MODEL

Convinced that the computations by themselves introduce no considerable error, we are in the position to test the accuracy of the slab model itself. To this effect the computations of Sec. III were repeated with 67, 51, 34 and 26 slabs, respectively. While there is no noticeable change in the heating efficiency η , the maximum departure in the value of $\langle P_{diss} \rangle$ from the mean is 3o %. Therefore, the results may be considered accurate within a factor of two for $\langle P_{diss} \rangle$ and exact for η .

VI. DISCUSSION AND CONCLUSIONS

In the representative case (Sec. III), the average dissipation in the plasma is 2.8×10^{-6} watt/cm^3 for a vacuum field of 1 volt/cm just outside the plasma boundary. For an acceptable vacuum field of 3ooo volt/cm, $\langle P_{diss} \rangle = 25$ watt/cm^3 which is adequate for the fusion requirements. The maximum field in the plasma then corresponds to 10^6 volt/cm which, of course, is absurd considering the linearized treatment.

It is found that considerable absorption at the LHR can take place even at high temperatures ($T = 10^8$ °K, $\langle \nu_{ei} \rangle / \omega = 10^{-7}$).

The problem expected from the non-fulfilment of the accessibility condition $n_z > 2$ is conspicuous by its absence. This discounts the apprehension that for the LH heating to make sense it is essential that the accessibility condition be satisfied [8] (see footnote 4).

It is found (Sec.IIIc) that even at the hybrid layer, the ions carry only half of the wave energy belying the expectations that the LH resonance could impart energy to the ions preferentially. A still closer examination of the collisional energy absorption would show that the ratio of the energy absorbed by the ions and the electrons is $\sqrt{\varepsilon_i \, m / \varepsilon_e \, M}$. Thus in the present case ($\varepsilon_i = \varepsilon_e$), almost 98 % of the dissipation is accounted for by electron heating while only 2 % of the energy goes into heating the ions. At

fusion parameters, however, ions would get heated by collisions with electrons. Also direct ion heating by collisionless cyclotron-harmonic absorption (specially in the presence of magnetic field gradients in a torus) is not to be ruled out.

Perhaps the most important conclusion to be drawn from this work is that rf energy can by readily coupled and efficiently absorbed even in the presence of weak absorption mechanisms.

ACKNOWLEDGEMENTS

The successful execution of this work owes itself to the tireless dedication of Frau Stöckermann, who carried out the extensive computations spanning the period of over a year. Dr. John Tataronis suggested the use of iterative methods for solving transcendental equations and rewrote the rootfinding routine with complex quantities. In addition, helpful discussions were held with Dr. H. Derfler, Dr. F. Leuterer, Dr. H. M. Mayer and Dr. J. Tataronis. To all of these people we express our sincere gratitude.

FOOTNOTES

1 Even before this work was undertaken Derfler, realising that in a fusion plasma the characteristic rf wavelengths would become comparable to the radial plasma dimensions, had proposed the construction of slow wave structures inside the vacuum vessel with a view to obtain large k_z in order to create the necessary conditions for collisionless Landau damping /12/. The idea to treat the LH heating as an eigenvalue problem inside a waveguide is due to the present authors, however.

2 An exhaustive discussion of plasma filled waveguides is to be found in Ref. 13.

3 The Langevin collision model is identical to the collision tensor in the hydromagnetic equations given in Ref.2, p.252.

4 Lack of accessibility into the plasma results in almost complete reflection (say 9o %) of the wave energy incident on the plasma surface from the vacuum region. However, precisely due to the same effect in reverse, the 1o % energy entering the plasma is trapped inside the plasma. One can readily verify that after a few reflections between the plasma boundary and the metallic wall, a large portion of the original wave energy has entered the plasma until an equilibrium is established between the energy fluxes

leaving and entering the plasma. Given a better possibility of dissipation in the plasma as compared to the metallic wall, it stands to reason that a high heating efficiency is obtained. The eigenvalue solution, however, does not directly expose the role of the accessibility condition and the results quoted in this paper are valid only in the absence of transients.

REFERENCES

[1] BUDDEN, K.G., Proc. Roy. Soc. A227 (1955) 516

[2] STIX, T. H., Theory of Plasma Waves, McGraw Hill, New York (1962) 24o - 244

[3] GINZBURG, W. L., Propagation of Electromagnetic Waves in a Plasma, Moscow (196o)

[4] STIX, T. H., Phys. of Fluids 3 (196o) 19

[5] STIX, T. H., Phys. Rev. Letters 15 (1965) 878

[6] DOLGOPOLOV, V. V., Zh. Tekh. Fiz. 36 (1963) 273, Sov. Phys. Tech. Phys. 11 (1966) 198

[7] AGNELLO, V., COLOMBANT, D., FIEFFE-PREVOST, P., ICHTCHENKO, G., KULINSKI, S., IV-ECCFPD, Rome (197o) 131

[8] PARKER, R., QPR No. 1o", Research Lab. of Electronics, Massachusetts Institute of Technology, Cambridge, Massachusetts, USA (1971) 97 - 111

[9] HOOKE, W.M., BERNABEI, S., KINDEL, J.M., LEE, Y.C., American Physical Society Bulletin (1971) 1278

[10] PEŠIĆ, S. S., Nuclear Fusion 11 (1971) 461

[11] GLAGOLEV, V. M., Plasma Physics 14 (1972) 315

[12] DERFLER, H., communicated to the "Advisory Group on Plasma Heating", Grenoble (March 29 - 31, 1971)

[13] ALLIS, W. P., BUCHSBAUM, S.J., BERS, A., Waves in Anisotropic Plasmas, MIT Press, Cambridge, Massachusetts (1963)

[14] SPITZER, L., Physics of Fully Ionized Gases, Interscience Publishers, New York (1962) 137 - 139

Table I

Plasma-column half-width "a"	10 cm
Waveguide half-width "b"	20 cm
Plasma-profile width "g"	1 cm
Magnetic field "B_o"	100 kG
Ion-cyclotron frequency "f_{ci}"	$.76 \times 10^{8}$ Hz
RF frequency "f"	$.76 \times 10^{9}$ Hz
Plasma density at the lower -hybrid resonance "n_{lh}"	2.7×10^{13} cm^{-3}
Maximum plasma density "n_{max}"	3.5×10^{13} cm^{-3}
Temperature "T"	3×10^{4} °K
and the corresponding relative collision frequency, $\langle \nu_{ei} \rangle / \omega$	10^{-2}
Gas used	Deuterium
Wall material	Stainless steel
Number of plasma slabs	199

The parameters used in the representative case studied in Sec. III.

Table II

Mode	n_z	k_z cm^{-1}	λ_{abs} cm	$\langle P_{diss} \rangle$ watt cm^{-3}	η %
Symmetric	1.+i0.005	0.16+i0.0008	1500	2.8×10^{-6}	99.8
	0.8+i0.04	0.13+i0.006	170	3.3×10^{-2}	99.9
	0.5+i0.03	0.08+i0.004	250	14.0	99.9
Anti-Symmetric	0.99+i0.004	0.16+i0.0007	1400	2.3×10^{-6}	99.7
	0.75+i0.02	0.12+i0.004	300	0.12	99.9

Eigenvalues n_z (k_z), absorption length, average power dissipation and heating efficiency for the five propagating eigenmodes for the parameters of Table I.

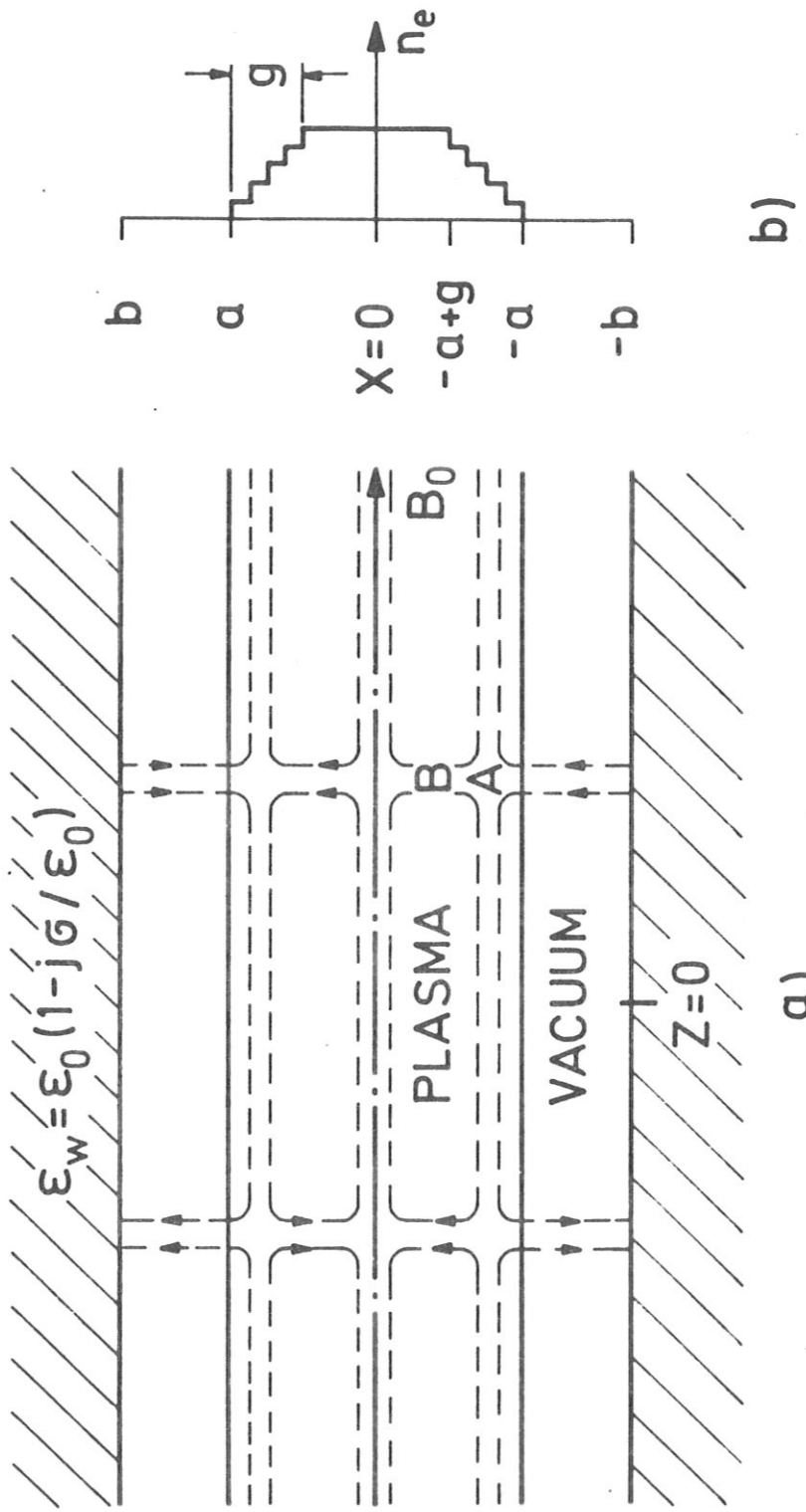

Fig. 1 The plasma filled parallel-plate waveguide. The electric field configuration for a symmetrig eigenmode is shown by the dashed lines.

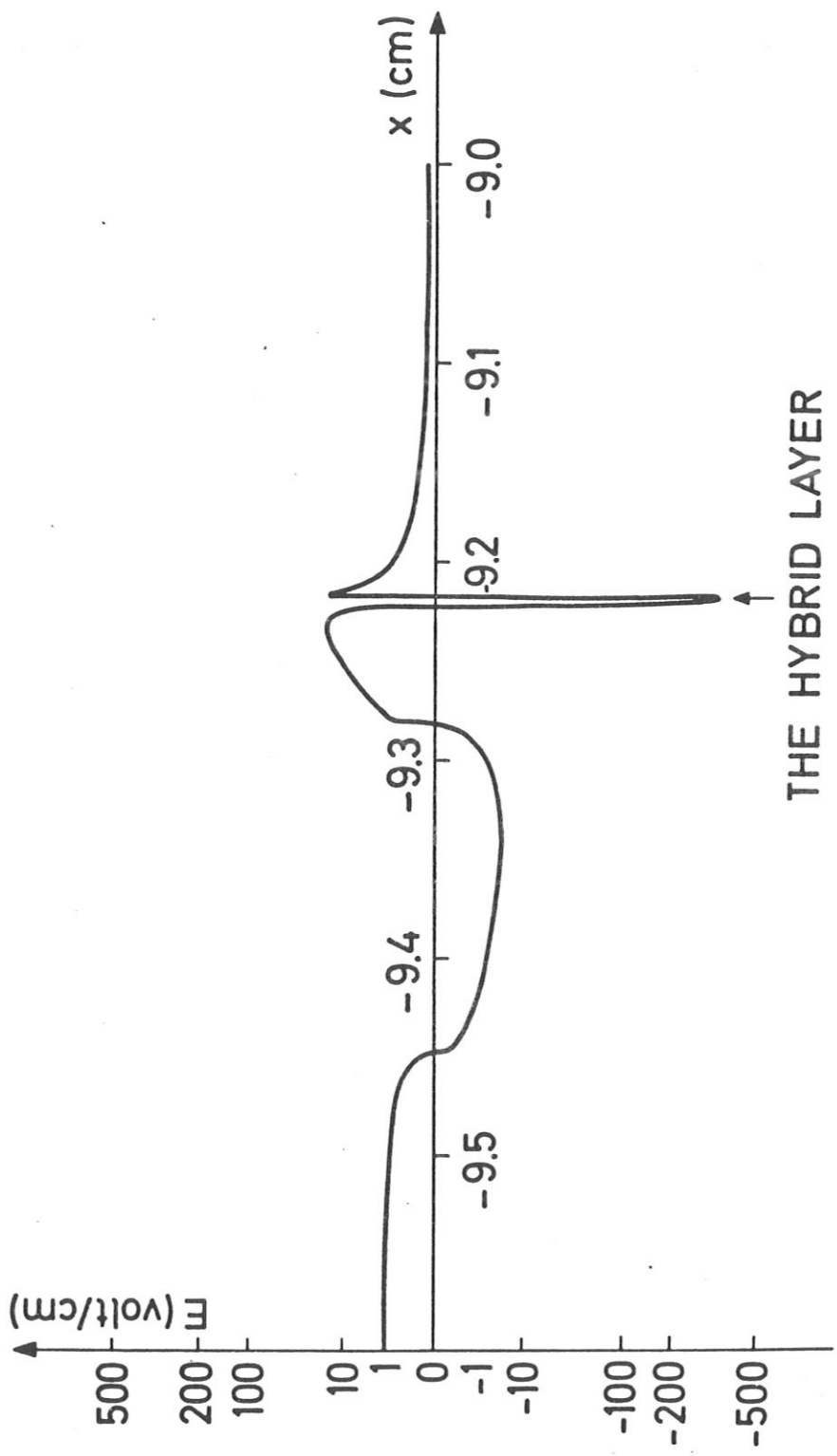

Fig. 2 Electric field as a function of position at a particular instant. The peculiar distortion is due to the cubic compression of the vertical scale.

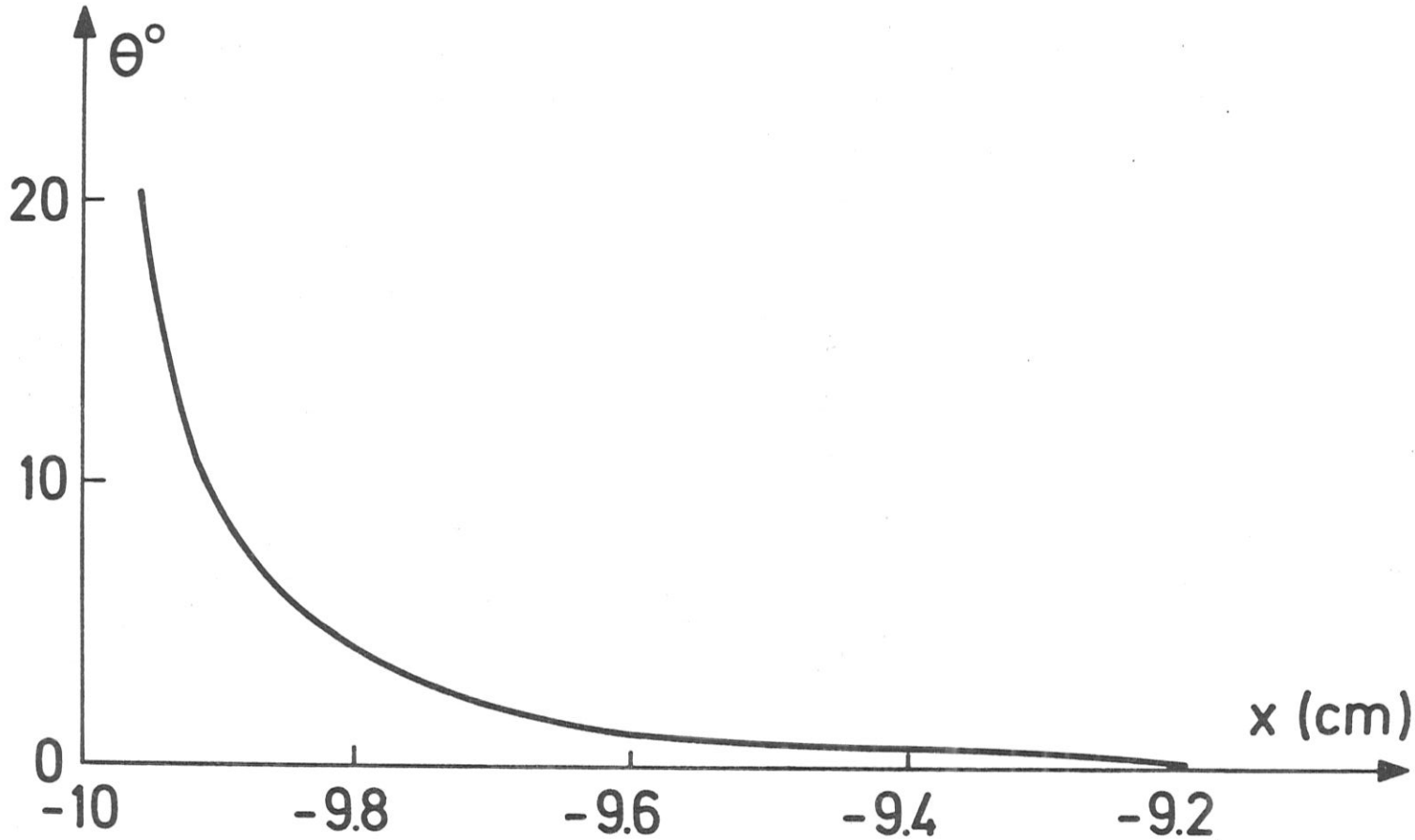

Fig. 3 The angle between the electric field and the propagation direction of the slow wave. This angle decreases monotonically as the hybrid resonance is approached and the wave assumes an electrostatic character.

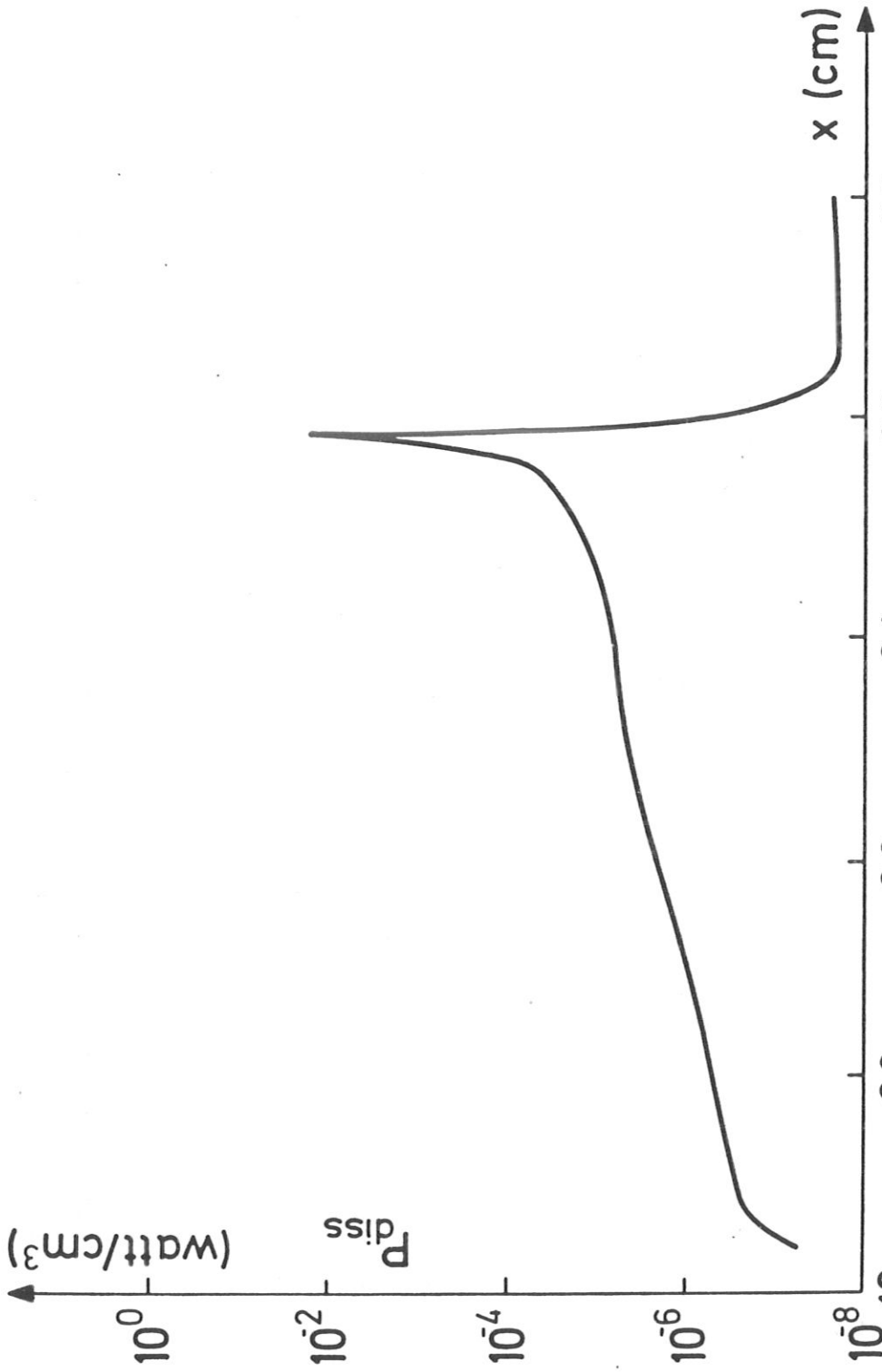

Abb. 4 Dissipation per unit volume as a function of position.

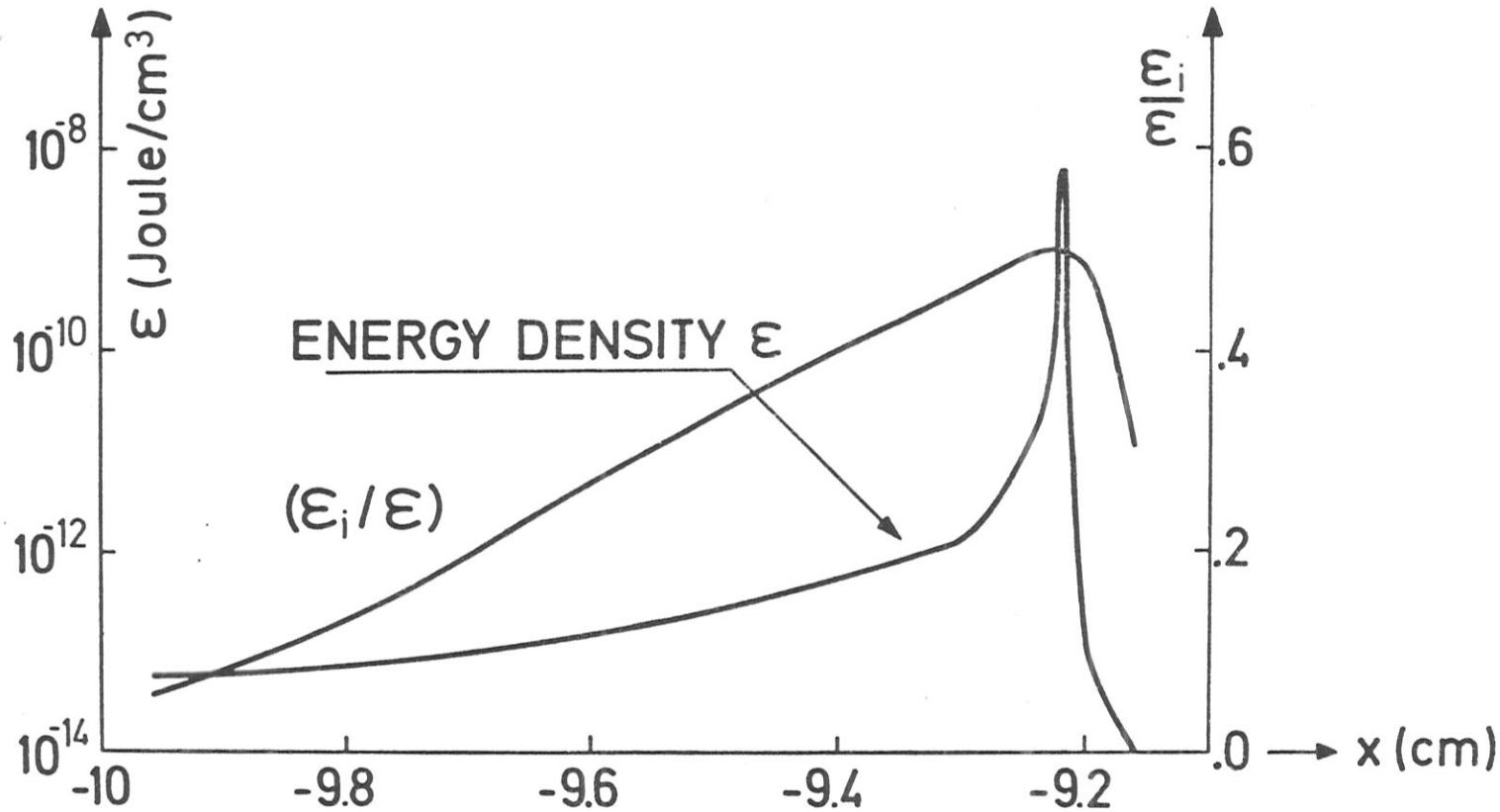

Fig. 5 Total energy density and the ratio of ion to electron energy density as a function of position.

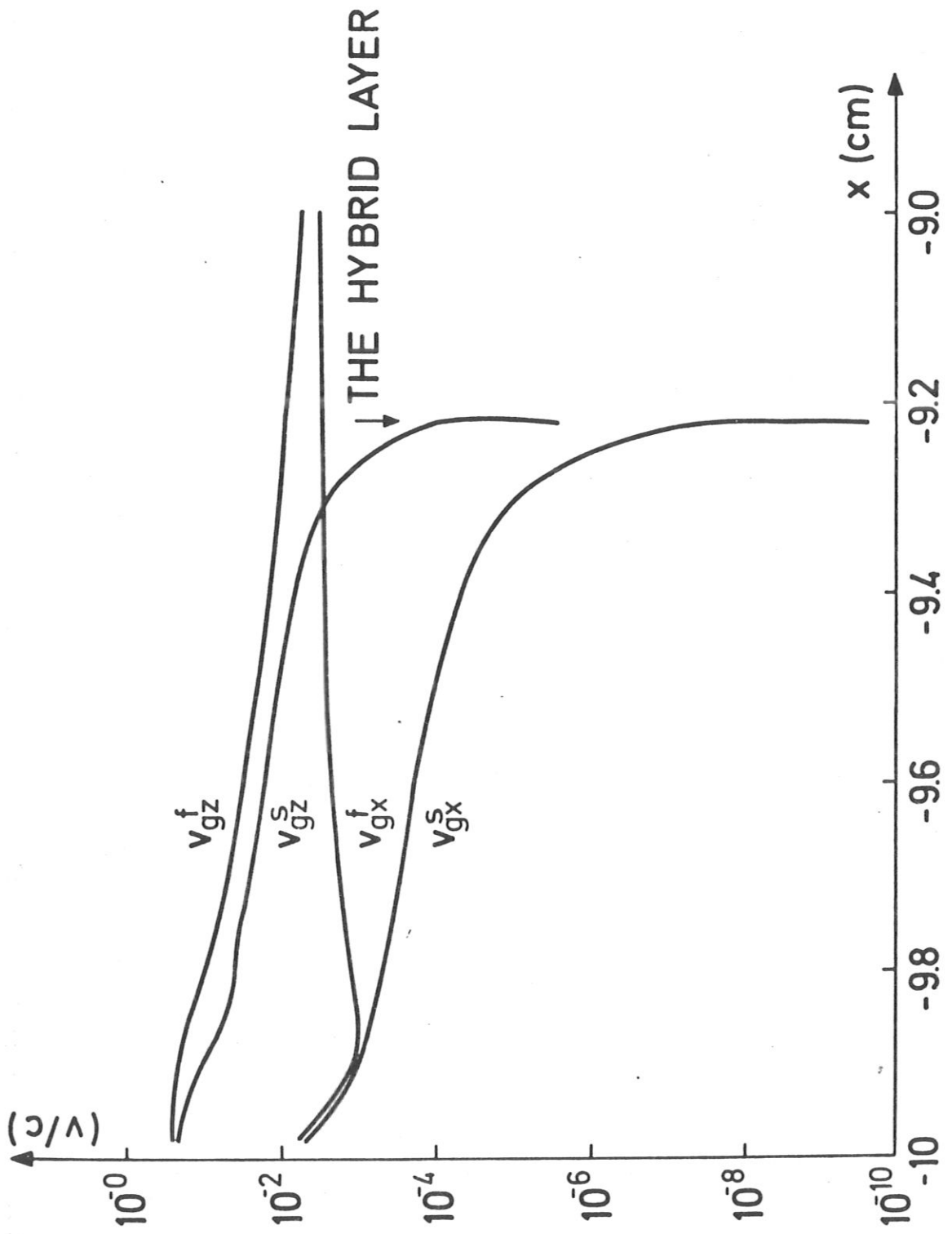

Fig. 6 Group velocity as a function of position.

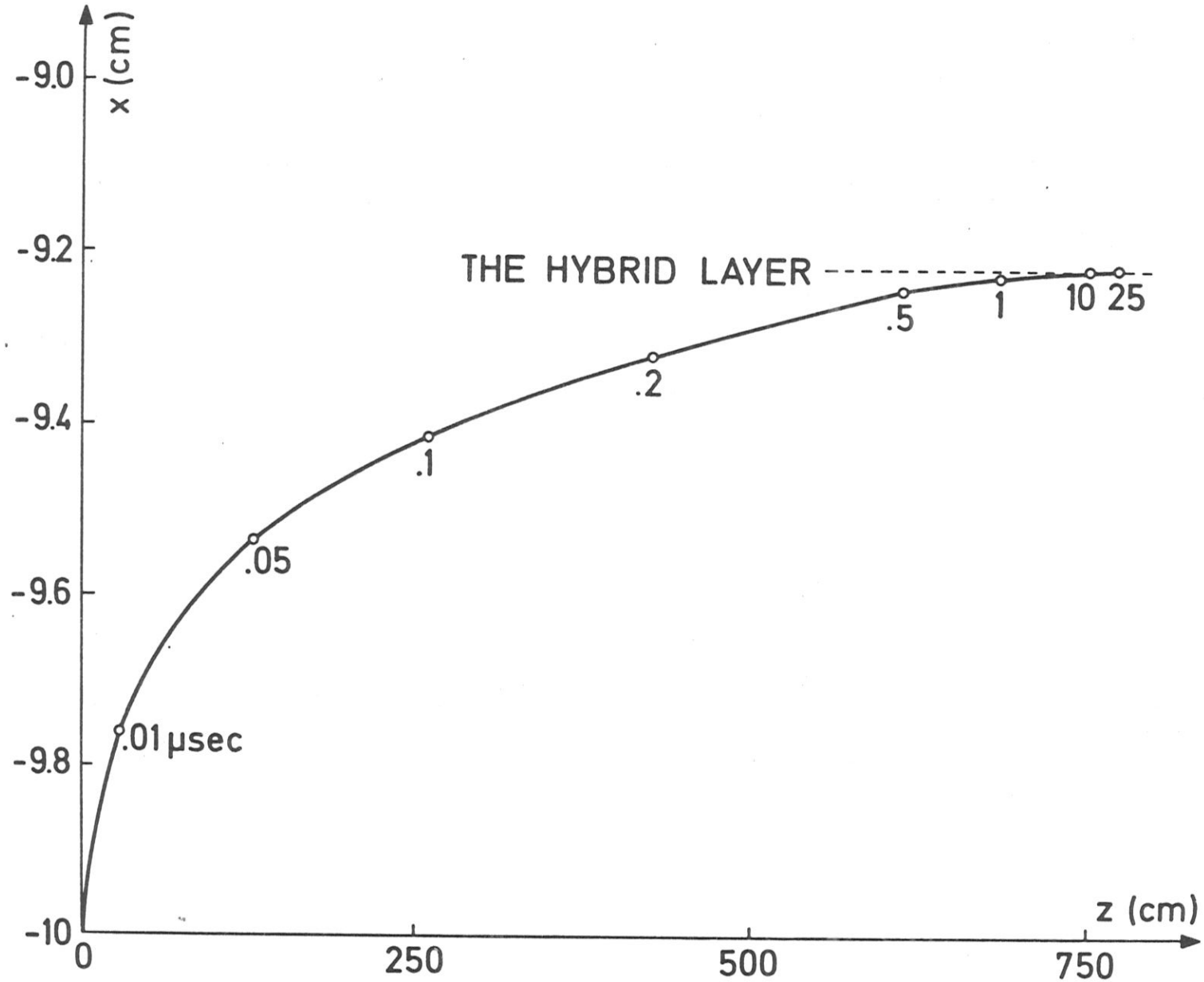

Fig. 7 Propagation of an energy pulse (travelling at the group velocity of the slow wave) from the plasma boundary to the hybrid layer.

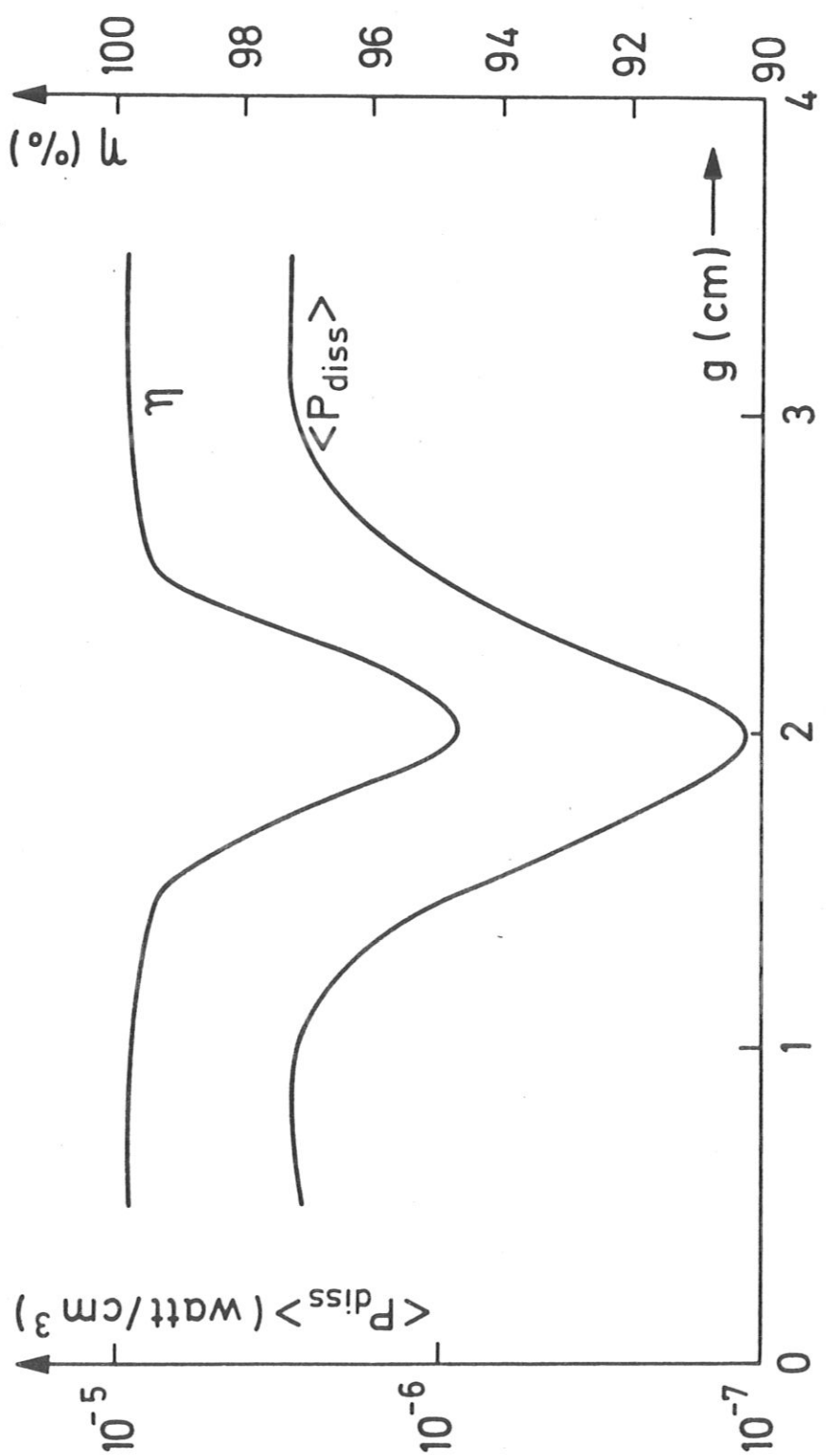

Fig. 8 Average dissipation density and heating efficiency as a function of plasma profile width "g".

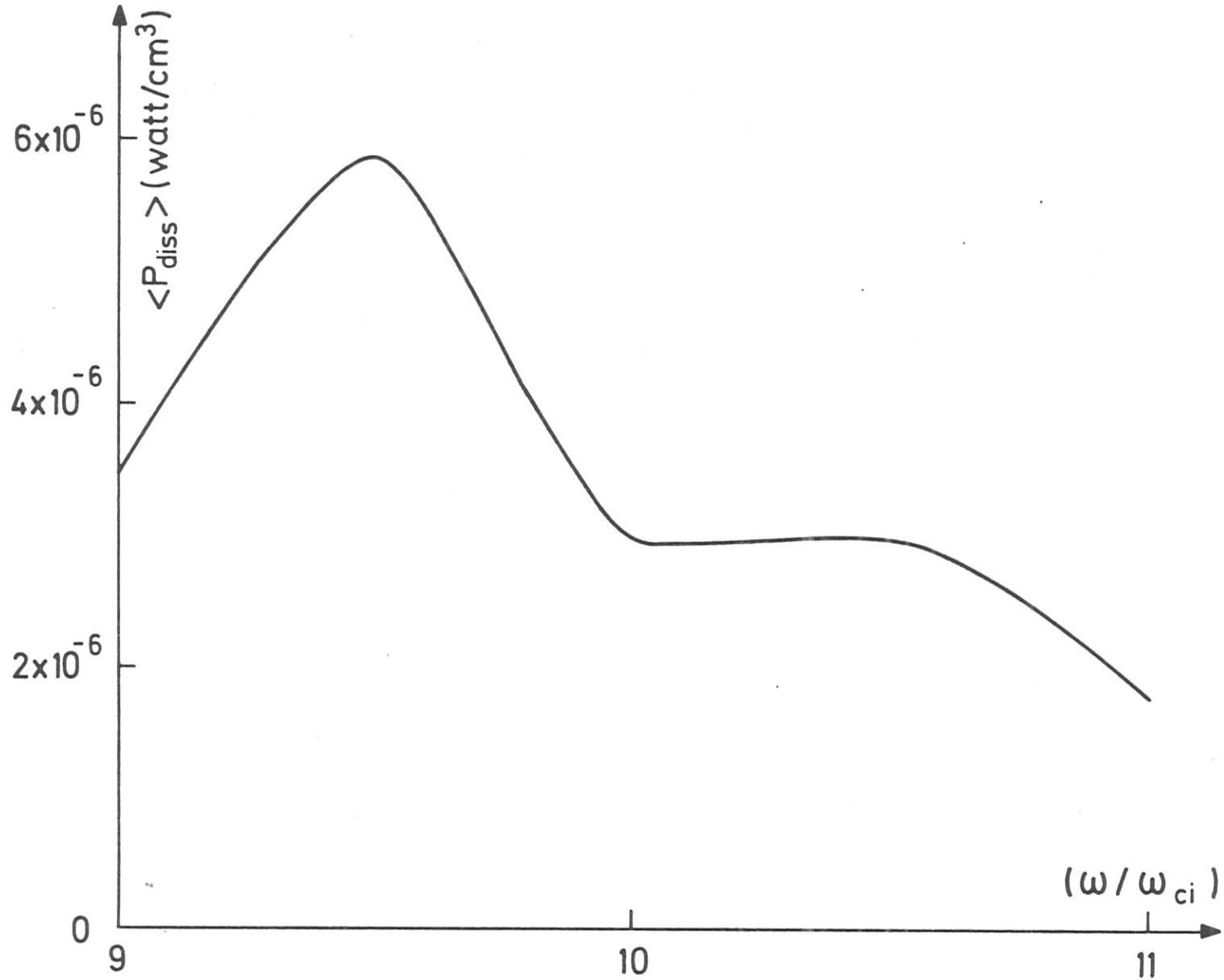

Fig. 9 Average dissipation density and heating efficiency as a function of frequency.

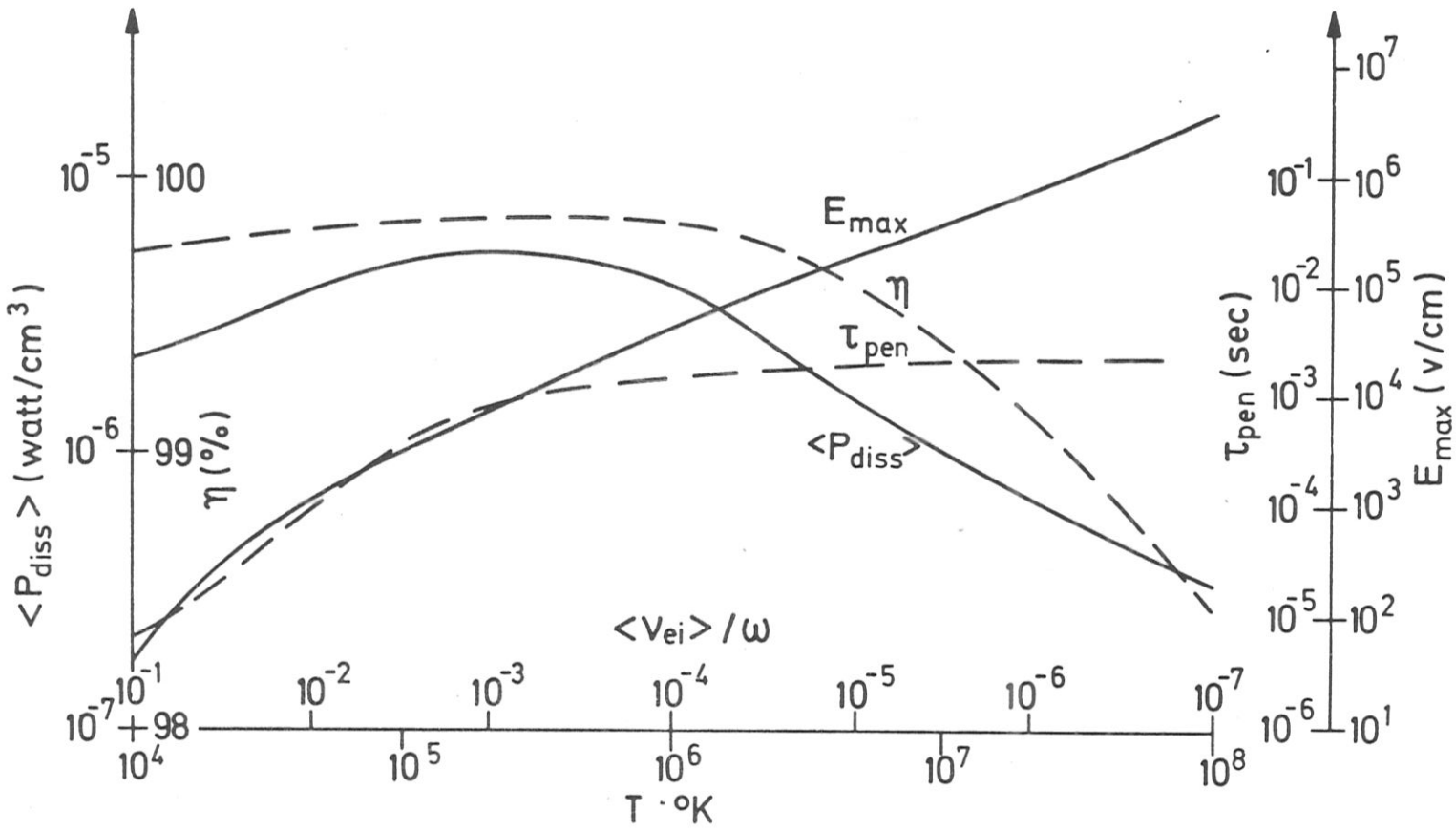

Fig. 1o Average dissipation density, heating efficiency, maximum electric field in the plasma and energy penetration time as a function of the collision frequency.